Astrophysical S factor for α-capture on ^{112}Sn in the p-process energy range

N. Özkan,* G. Efe, and R. T. Güray
Kocaeli University, Department of Physics, Umuttepe TR-41380, Kocaeli, Turkey

A. Palumbo, J. Görres, H. Y. Lee, L. O. Lamm, W. Rapp, E. Stech, and M. Wiescher
University of Notre Dame, Department of Physics, Notre Dame, Indiana 46556, USA

Gy. Gyürky, Zs. Fülöp, and E. Somorjai
Institute of Nuclear Research (ATOMKI), H-4001 Debrecen, P. O. Box 51., Hungary
(Received 20 October 2006; published 8 February 2007)

The cross section of the reaction ^{112}Sn$(\alpha, \gamma)^{116}$Te has been measured in the energy range of astrophysical interest for the p-process. Highly enriched self-supporting ^{112}Sn foils were bombarded with α beams in the effective center of mass energy range from 7.59 to 11.42 MeV at the Notre Dame FN Tandem Van de Graaff accelerator. The characteristic activity of ^{116}Te was counted with a pair of large volume Ge clover detectors in close geometry to maximize the detection efficiency. The cross section of the concurrent (α, p) reaction has also been measured. The results are compared with statistical model predictions for different global α-nucleus potentials.

DOI: 10.1103/PhysRevC.75.025801 PACS number(s): 25.55.−e, 26.30.+k, 27.60.+j

I. INTRODUCTION

The elements heavier than iron are mainly synthesized by two mechanisms: the slow neutron capture process (s-process) and the rapid neutron capture process (r-process). An additional mechanism, the p process, is responsible for the production of 35 proton-rich stable isotopes whose abundance accounts typically for less than 1% of the total isotopic abundances. These so-called p nuclei between Se and Hg are shielded by stable nuclei from the production via the s and r-processes.

The p-process can proceed via a combination of photodisintegration reactions, (γ, n), (γ, p), and (γ, α), on existing heavy s and r seeds in the temperature range of 2–3 GK. These high temperatures can be achieved in explosive environments, such as the O/Ne layers of Type II supernovae [1,2]. Initially, the nuclides are driven by a sequence of (γ, n) reactions toward the proton-rich side where the binding energies of neutrons become gradually larger along the isotopic path. When the (γ, p) and/or (γ, α) reactions become faster than (γ, n) reactions, the reaction path branches as seen in Fig. 1 [3,4] and the (γ, p) and (γ, α) reactions may play an important role in determining the final p-nuclei abundances in this mass range. The p-process and possible p-process sites have been reviewed in detail in Ref. [5].

Although a large reaction network of several hundreds to thousands of reaction rates involving stable as well as unstable proton-rich nuclei is required to describe the p-process nucleosynthesis, not much experimental effort has been devoted to relevant nuclear cross-section determination. Most γ-induced reactions are very difficult to measure directly [6]. Instead, the charged-particle-induced reaction cross sections can be measured and its inverse photodisintegration reaction cross sections are calculated using the detailed balance theorem, which is only valid if all nuclei involved are fully thermalized [7]. Experimental data for the charged-particle-induced reaction cross sections are scarce above Fe. To date, more proton capture versus α-capture reaction cross sections have been measured [8–18]. This is due to the fact that the corresponding energies for α-capture reactions are well below the Coulomb barrier, making the cross sections small. Experimental aspects for the measurements of the p-process reactions are discussed in Refs. [19,20], whereas results of the α-capture on ^{63}Cu, ^{70}Ge, ^{96}Ru, ^{106}Cd, ^{112}Sn, ^{118}Sn, and ^{144}Sm can be found in Refs. [21–27], respectively.

P-process studies are based mostly on Hauser-Feshbach statistical models to predict the reaction rates. Although the (p, γ) measurements generally agree with the statistical model predictions within less than a factor of 2, (α, γ) measurements show considerable underestimation compared to their model predictions [27]. For the recent ^{106}Cd [24] measurements, the (α, γ) results are lower, whereas the (α, p) results are higher than the predictions. For the previously measured two (α, γ) data points on ^{112}Sn [25], only the higher energy value is in good agreement. The measurement of ^{112}Sn$(\alpha, \gamma)^{116}$Te is very important because different optical potentials result in different S-factor predictions as given in Ref. [28]. It is, therefore, crucial to investigate the α-induced reaction cross sections experimentally to test the reliability of the statistical model predictions.

The scope of this article is to extend the experimental database and energy range by measuring the (α, γ) cross section on the p-nucleus ^{112}Sn with higher precision. In addition, this reaction has special importance for the study of photodisintegration leading to proton closed-shell nucleus, ^{112}Sn with $Z = 50$. The level density at closed shells is reduced and the Hauser-Feshbach statistical models may not work well; therefore, the ^{112}Sn$(\alpha, \gamma)^{116}$Te reaction is one of the best candidates to test the applicability of statistical

*Electronic address: nozkan@kou.edu.tr

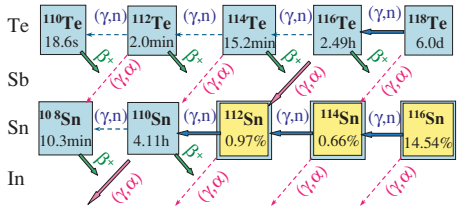

FIG. 1. (Color online) The relevant *p*-process reaction flow path around Sn isotopes. Because only even-even isotopes are shown, (γ, n) arrows indicates two subsequent (γ, n) reactions. The main and weaker flow paths are shown by solid and dashed arrows, respectively. Stable isotopes are represented by double squares indicating the isotopic abundances and unstable ones by squares with their half-lives.

models at closed shells. In the present work, the cross-section measurements and the deduced *S* factors are compared with NON-SMOKER statistical model results calculated with the standard input parameter set [29]. The details of the experimental procedure [30] and the experimental results are presented and discussed as follows.

II. MEASUREMENTS

The ^{112}Sn$(\alpha, \gamma)^{116}$Te reaction cross sections have been measured via the activation technique in the effective center-of-mass energy range $7.59\,\text{MeV} \leqslant E^{\text{eff}}_{\text{c.m.}} \leqslant 11.42\,\text{MeV}$ at the FN Tandem Van de Graaff accelerator at the University of Notre Dame, USA. These energies are particularly interesting because the Gamow window for the ^{112}Sn$(\alpha, \gamma)^{116}$Te reaction at 3 GK is between 6.86 and 10.3 MeV and the Gamow peak is at 8.58 MeV. In addition, the ^{112}Sn$(\alpha, p)^{115}$Sb reaction cross sections have been investigated in the 9.97–11.42 MeV energy range. The ^{112}Sn$(\alpha, n)^{115}$Te reaction cross sections cannot be measured because the (α, n) channel is not open within the studied energy range.

The activation technique involves the bombarding of a target with projectiles to produce radioactive species and the measurement of their specific γ activities after the irradiation has stopped. The details of the activation method and data analysis can be found in Ref. [25].

For α-induced reactions on ^{112}Sn, the activation technique is an appropriate technique to determine the cross sections because the reaction products are radioactive with convenient half-lives ($t_{1/2}$ = 2.49 h for ^{116}Te and 32.1 min for ^{115}Sb) and branchings as given in Table I. The relevant part of the table of isotopes and the flow path around the Sn isotopes are shown in Fig. 1.

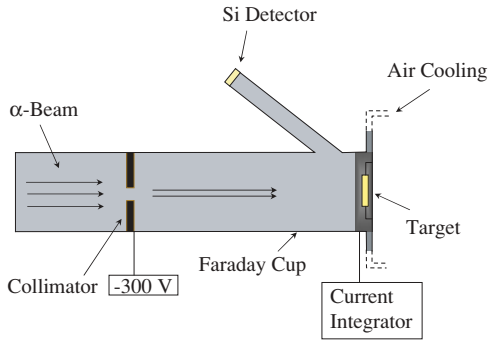

FIG. 2. (Color online) A drawing of the components used in the beam line during the irradiation. The beam was defined by a collimator with a diameter of 5 mm. The target was placed at the end of the beam line and Si detector at 135° with respect to beam direction for RBS measurements [30].

A. Targets

Isotopically enriched ^{112}Sn targets in the form of thin self supporting foils of 2.2 mg/cm^2 were used in this experiment. The highly enriched (99.60%) ^{112}Sn targets were prepared at Argonne National Laboratory via mechanical rolling [30].

The ^{112}Sn foils were mounted on Ta frames with hole diameters of 12.5 mm. The target thickness was determined by Rutherford back scattering (RBS) to be $2.2 \pm 0.2\,\text{mg/cm}^2$ and was verified at the end of the experiment. The target stability was also monitored continuously by detecting the backscattered α particles from the target. For this purpose a collimated silicon surface barrier detector was mounted at 135° with respect to the beam direction during the irradiation as shown in Fig. 2.

Before the measurements, test runs were done with natural Sn targets to find out how much α-beam current can be applied. These tests showed that there was no deterioration with α-beam currents of up to 300 nA.

B. Activations

^{112}Sn targets were irradiated with an α-beam (^{4}He^{++}) starting from the effective center of mass energy $E^{\text{eff}}_{\text{c.m.}}$ = 7.59 MeV increasing by 0.50 MeV lab energy steps. Below 7.59 MeV, no data could be obtained due to the low count rate.

A diagram of the experimental setup for the target irradiation is shown in Fig. 2. The target was placed in a brass holder. Due to the relatively low melting point of ^{112}Sn, the brass target holder was air cooled during the irradiation to prevent target degradation. A thick carbon foil was placed directly behind

TABLE I. Decay parameters of the ^{112}Sn + α reaction products taken from the literature [31,32].

Nuclear reaction and related decay products	Half-life	γ energy (keV)	I_γ (%) relative intensity per decay
^{112}Sn$(\alpha, \gamma)^{116}$Te$(\beta^+)^{116}$Sb	2.49 ± 0.04 h	628.7, 637.9	3.21 ± 1.5, 0.75 ± 0.04
^{116}Sb$(\beta^+)^{116}$Sn	15.8 ± 0.8 min	931.8, 1293.6, 2225.2	24.8 ± 1.9, 85 ± 6, 14.6 ± 1.3
^{112}Sn$(\alpha, p)^{115}$Sb$(\beta^+)^{115}$Sn	32.1 ± 0.3 min	497.3	97.9

the target to stop the beam. To get an accurate measurement of the total number of charged particles hitting the target during the irradiation runs, the entire target chamber was designed as a Faraday cup, isolated from the rest of the beam line. Secondary electrons from the target were suppressed by a bias voltage of −300 V. The beam current was recorded in real time with a current integrator in time steps of 32 s, allowing fluctuations in the beam to be monitored. Throughout the irradiations with different α-beam energies, the typical current was between 200 and 250 nA.

The length of irradiation was chosen based on the half-life of the (α, γ) activation product, in the range of 30 min and 6 h (approximately 3 half-lives). Due to the steeply decreasing cross sections at low beam energies, the longer irradiation time was applied for low-energy measurements.

C. Gamma counting and analysis

After each irradiation, the target was taken to a separate low-background counting area to measure the ^{116}Te and ^{115}Sb activities produced through the ^{112}Sn$(\alpha, \gamma)^{116}$Te and ^{112}Sn$(\alpha, p)^{115}$Sb reactions.

The detection system was composed of two Clover Ge detectors (Clover 1 and Clover 2). Each detector has four individual HPGe crystals with a relative efficiency of 20% at a γ energy of 1.33 MeV. Figure 3 shows the arrangement of detectors and the position of the activated sample in the counting setup. To be able to measure the induced γ-ray activity at α energies as low as possible, the Clover Ge detectors were placed face to face in close geometry. The distance between the detector end caps was fixed at 4.9 mm for reproducibility of the counting geometry. To reduce the room background, the detectors were shielded with 5 cm of Pb and an inner Cu lining of 3 mm. After each irradiation, the activated target was placed at the center of the detectors and positioned at their common axis. Depending on the count rate of the targets, the decays were observed in time intervals from 30 min to 7 h. For the dead-time correction (0.5−6%), the output signal of a fixed frequency (100 Hz) pulse generator was also fed into the electronics. To reduce the pileup and summing losses, each crystal was utilized as a single detection unit operating in "direct" mode as described by Ref. [33]. This implies that the

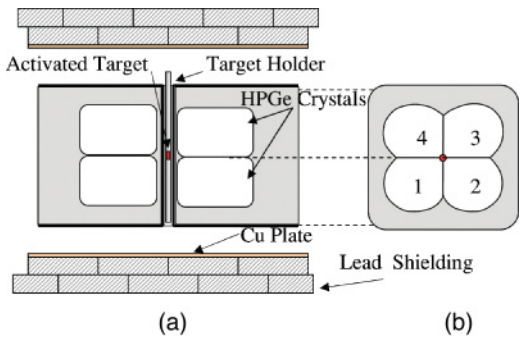

FIG. 3. (Color online) The scheme of experimental setup used to measure the induced γ-ray activity. (a) Low background counting area surrounded by Pb bricks and Cu plates. (b) Target position viewed from the front window of the Clover 2 [30].

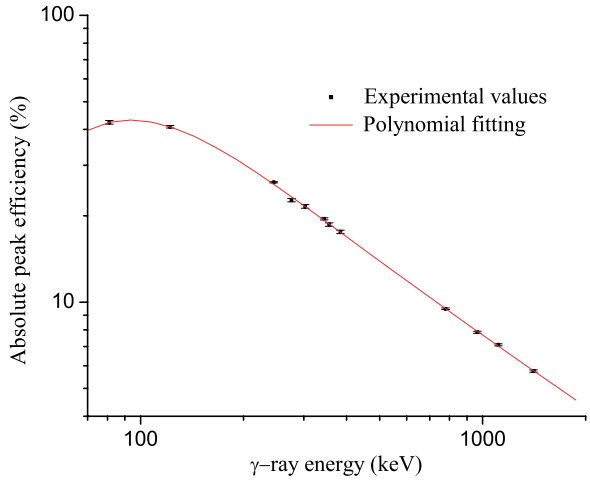

FIG. 4. (Color online) Measured absolute peak efficiency curve for the double Clover detection system. The data is fitted with a fifth-order polynomial function ($\chi^2 = 0.9997$).

photopeak detection efficiency of the system was the sum of the individual photopeak efficiencies of each crystal (eight crystals in all). The nearly 4π detection geometry offers relatively high efficiency (see Fig. 4), enabling detection of γ peaks at low irradiation energies where the cross sections are low.

The absolute photopeak efficiencies of the detectors were determined by the efficiency-ratio method using an uncalibrated ^{152}Eu source and calibrated ^{54}Mn, ^{60}Co, and ^{133}Ba sources. This method requires a knowledge of the relative emission probabilities of the source of unknown activity and at least one energy to be in an energy range for which the absolute efficiency has already been determined [34]. The set of relative efficiency values (relative to 122 keV γ efficiency) obtained with the ^{152}Eu source was normalized to fit in with known efficiency values obtained with ^{54}Mn, ^{60}Co, and ^{133}Ba sources. The presence of cascade transitions requires coincidence-summing corrections that cannot be ignored because of the close geometry. Summing correction factors were calculated using "summing coefficients" taken from Ref. [35]. Figure 4 depicts the measured absolute photopeak efficiency calibration points for the double Clover detection system. The photopeak efficiency, for example, is $(8.1 \pm 0.2)\%$ for the 932 keV γ-line.

As an alternative, the coincidence method was used to check the reliability of the detection efficiency calibration. This method is based on counting photons coincident with others in a selected cascade transition. Using this method, absolute photopeak efficiencies can be obtained without knowing the source strength and summing correction [34]. Due to the close geometry, corrections for angular distribution effects were negligible. Both coincidence and efficiency-ratio methods agreed within the uncertainties.

III. RESULTS AND COMPARISON WITH HF PREDICTIONS

The cross section and the S-factor results are obtained in this work for ^{112}Sn$(\alpha, \gamma)^{116}$Te and ^{112}Sn$(\alpha, p)^{115}$Sb reactions.

For the ^{112}Sn$(\alpha, \gamma)^{116}$Te reaction, we were able to measure cross sections from parent and daughter decays because both

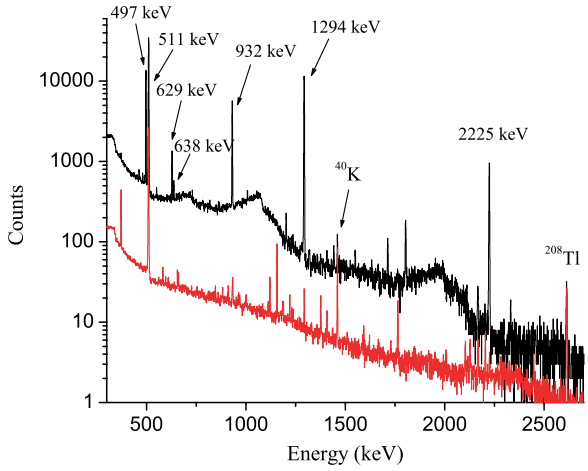

FIG. 5. (Color online) The γ-ray spectrum in the relevant energy region obtained after the irradiation with α beam of $E^{\text{eff}}_{\text{c.m.}} = 11.42$ MeV (the upper spectrum) for the counting time of 30 min. The lower spectrum shows the γ-ray spectrum obtained with α beam of $E^{\text{eff}}_{\text{c.m.}} = 8.06$ MeV normalized to 30 min. The γ-lines used for cross-section measurements are indicated by arrows with corresponding energy values.

the parent nucleus ^{116}Te and the daughter nucleus ^{116}Sb are radioactive, as seen in Table I. As examples, the γ-ray spectra for the ^{112}Sn(α, γ)^{116}Te reaction obtained at $E^{\text{eff}}_{\text{c.m.}} = 8.06$ MeV and $E^{\text{eff}}_{\text{c.m.}} = 11.42$ MeV α-beam irradiation are presented in Fig. 5. Because the characteristic γ transitions of 629 and 638 keV in ^{116}Sb populated through the β^+ decay of the reaction product ^{116}Te have small branching ratios (Table I), the cross sections were measured in the α-beam energy range 9.01 MeV $\leqslant E^{\text{eff}}_{\text{c.m.}} \leqslant$ 11.42 MeV. For α-beam energies below $E^{\text{eff}}_{\text{c.m.}} = 9.01$ MeV, γ transitions of 932 and 1294 keV in ^{116}Sn populated by the ^{116}Sb secondary β^+ decay were observed with sufficient yields. For the lowest beam energy value of $E^{\text{eff}}_{\text{c.m.}} = 7.59$ MeV, we were only able to identify the 1294-keV line with good-enough statistics for the analysis. The γ transitions of 2225 keV from the daughter decay was not

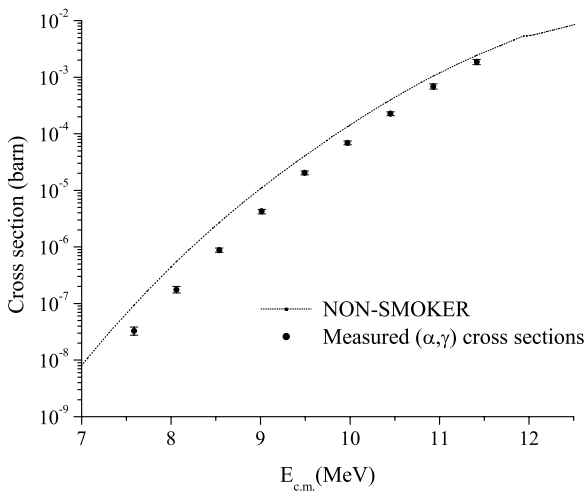

FIG. 6. The cross sections of ^{112}Sn(α, γ)^{116}Te reaction compared with the NON-SMOKER calculations (solid line) [29].

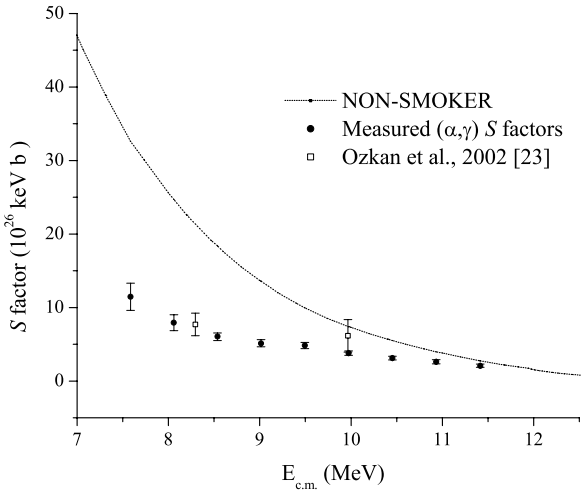

FIG. 7. The S factors of ^{112}Sn(α, γ)^{116}Te reaction compared with the NON-SMOKER calculations (solid line) [29]. The circles and the triangles represent the measured results and the previous data [25], respectively.

used because of the lower photopeak efficiency that resulted in a lower count rate even though it has a relatively high branching ratio (Table I). The cross sections resulting from the analysis of different γ-decay transitions for ^{112}Sn(α, γ)^{116}Te were found to be statistically consistent with each other [30]. As a result, the weighted averages of ^{112}Sn(α, γ)^{116}Te reaction cross section and S factor values were deduced from different γ-lines.

For the ^{112}Sn(α, p)^{115}Sb reaction, only one γ transition of 497 keV line in ^{115}Sn is populated through the β^+ decay of the reaction product ^{115}Sb. Cross sections for this reaction could be determined only in the α-beam energy range 9.97 MeV $\leqslant E^{\text{eff}}_{\text{c.m.}} \leqslant$ 11.42 MeV.

For the ^{112}Sn(α, γ)^{116}Te and ^{112}Sn(α, p)^{115}Sb reactions, the cross sections and S factors are shown in Figs. 6 and 7 and then 8 and 9, respectively. The values are also listed in

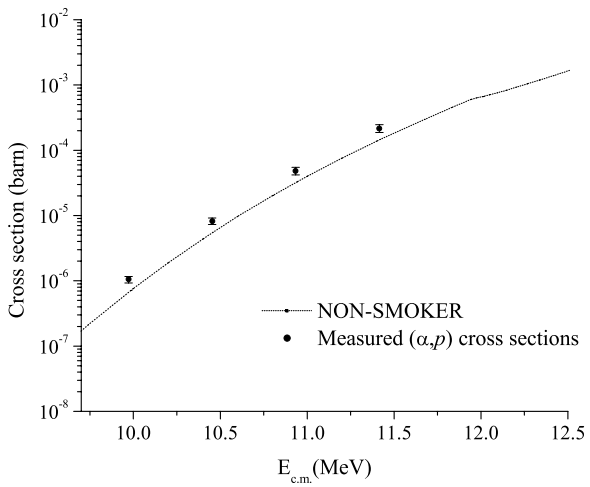

FIG. 8. The cross sections of ^{112}Sn(α, p)^{115}Sb reaction compared with the NON-SMOKER calculations (solid line) [29].

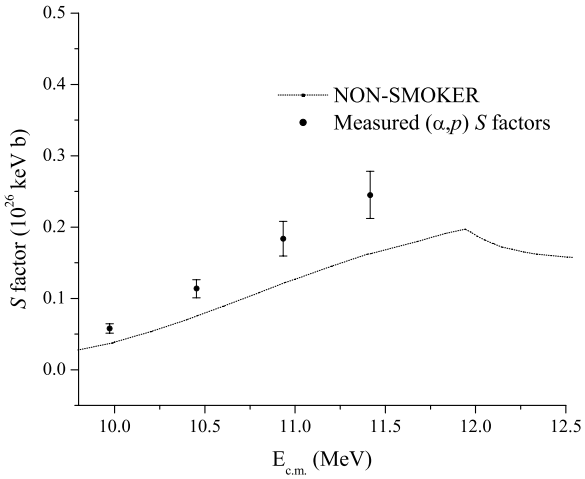

FIG. 9. The S factors of ^{112}Sn(α, p)^{115}Sb reaction compared with the NON-SMOKER calculations (solid line) [29].

Tables II and III, where the first and the second columns indicate the laboratory beam energies and the effective center-of-mass beam energies, respectively. The effective center of mass energy error is ∼1% due to the uncertainties in the effective energy calculation and the target thickness.

The total error of the measured cross section values includes two components: statistical error based on counting statistics of the analyzed γ-lines (between 0.2 and 25% depending on the bombarding energy) and systematical error based on the errors in the procedural techniques such as the error in the efficiency measurement (2%), the error in the beam current integration (2%), and target thickness (9%). These components were added in quadrature.

IV. DISCUSSION

The ^{112}Sn(α, γ)^{116}Te and ^{112}Sn(α, p)^{115}Sb reaction cross sections and S factors have been measured using the activation method in the energy range relevant to p-process. This energy range spans the Gamow window predicted for this reaction in the high temperature environment. The present results agree

TABLE II. Measured cross sections and S factors of the ^{112}Sn(α, γ)^{116}Te reaction.

E_{beam} (MeV)	$E^{\text{eff}}_{\text{c.m.}}$ (MeV)	Cross section ($\times 10^{-6}$ barn)	S factor ($\times 10^{26}$ keV b)
8.000	7.586	0.033 ± 0.005	11.5 ± 1.9
8.500	8.061	0.18 ± 0.02	7.94 ± 1.07
9.000	8.537	0.88 ± 0.07	6.0 ± 0.5
9.500	9.014	4.2 ± 0.4	5.1 ± 0.5
10.000	9.492	20 ± 2	4.8 ± 0.4
10.500	9.972	69 ± 5	3.8 ± 0.3
11.000	10.452	226 ± 18	3.1 ± 0.3
11.500	10.933	691 ± 74	2.6 ± 0.3
12.000	11.415	1860 ± 197	2.1 ± 0.2

TABLE III. Measured cross sections and S factors of the ^{112}Sn(α, p)^{115}Sb reaction.

E_{beam} (MeV)	$E^{\text{eff}}_{\text{c.m.}}$ (MeV)	Cross section ($\times 10^{-6}$ barn)	S factor ($\times 10^{26}$ keV b)
10.500	9.972	1.1 ± 0.1	0.058 ± 0.007
11.000	10.452	8.2 ± 0.9	0.11 ± 0.01
11.500	10.933	48 ± 6	0.18 ± 0.02
12.000	11.415	217 ± 29	0.25 ± 0.03

with the previous two data points [25] within the experimental uncertainties.

The measured results were compared with the NON-SMOKER statistical model code [29] calculations using the standard settings with the potential of Ref. [36]. The ^{112}Sn(α, p)^{115}Sb results are higher than the predicted results as in Figs. 8 and 9. Although an agreement is observed at higher energies for ^{112}Sn(α, γ)^{116}Te reaction, the experimental data deviate considerably in the lower energy range from the theoretical prediction as in Figs. 6 and 7. The comparison of the results with those of the recent study of α-induced reactions on ^{106}Cd [24] shows a similar behavior: the theoretical predictions overestimate the (α, γ) measurements and underestimate (α, p) measurements.

In addition, the astrophysical S factor results for ^{112}Sn(α, γ)^{116}Te and ^{112}Sn(α, p)^{115}Sb reactions are compared to the predictions provided by Galaviz *et al.* [28] using different global α-nucleus potentials (Fig. 10): the potential of Avrigeanu *et al.* [37], the potential of Fröhlich *et al.* [38], the potential of Demetriou *et al.* [39], the potential of McFadden *et al.* [36], and the potential of Galaviz *et al.* [28]. The latter potential was derived from α-elastic scattering data on ^{112}Sn.

For the (α, γ) reaction, except for the potential of Fröhlich [38], the calculations significantly overestimate the S factors by factors of 2−10; moreover, the energy dependence of the S factor is poorly described (Fig. 10). An exception is the potential of Demetriou [39]; scaling the absolute S factor

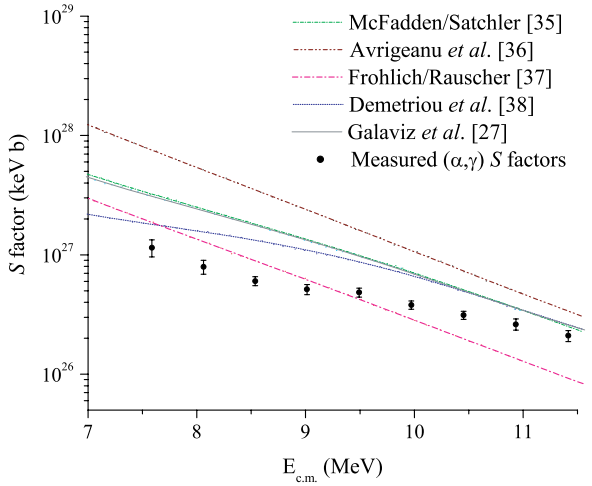

FIG. 10. (Color online) The S factors of ^{112}Sn(α, γ)^{116}Te reaction compared with the predictions from different global α-nucleus potentials, taken from Galaviz *et al.* [28].

with a factor of 1.8 reproduces the experimental data satisfactorily. This potential is based on a global fit of α-induced reaction cross sections for energies below 12 MeV in this mass range. However, it was pointed out by the authors that the predictive power was limited to within one order of magnitude.

Even though the α-potential of Galaviz *et al*. [28] was deduced from the elastic α scattering on ^{112}Sn, it only poorly describes the data for α-capture on ^{112}Sn. This might indicate that the deviation of the calculations from the experimental data is not only caused by the α-potential. New neutron- and proton-scattering data at energies that correspond to the same excitation range as for the α channel are necessary to elucidate the interplay between the different channels that seems to cause the observed discrepancies for the present reaction as well as for the case of ^{106}Cd+α [24].

The first steps for α-capture reaction measurements have been done; further experimental work, especially in the higher mass range, related to the α-induced reactions at energies around the Coulomb barrier is needed for *p*-process calculations. These values are crucial in determining the *p*-process path and branching points.

ACKNOWLEDGMENTS

The authors thank Daniel Galaviz (Michigan State University) and Thomas Rauscher (Universität Basel) for providing additional information on the impact of the α potential for the ^{112}Sn+α system. We acknowledge John P. Greene (Argonne National Laboratory) for preparing the ^{112}Sn targets for us. The assistance of C. Ugalde, E. Strandberg, A. Couture, and J. Couture (University of Notre Dame) during the experiment is highly appreciated. This work was supported by The Scientific and Technical Research Council of Turkey TUBITAK [grant TBAG-U/111 (104T2467)], the National Science Foundation NSF [grant 0434844], the Joint Institute for Nuclear Astrophysics JINA (www.JINAweb.org) PHY02-16783, and The Hungarian Scientific Research Fund Programs OTKA [grants T 42733, T 49245, F 43408, and D 48283]. Gy. Gy. and Zs. F. acknowledge support from the Bolyai grant.

[1] S. E. Woosley and W. M. Howard, Astrophys. J. Suppl. **36**, 285 (1978).
[2] M. Rayet, N. Prantzos, and M. Arnould, Astron. Astrophys. **227**, 271 (1990).
[3] T. Rauscher, Phys. Rev. C **73**, 015804 (2006).
[4] W. Rapp, J. Görres, M. Wiescher, H. Schatz, and F. Käppeler, Astrophys. J. **653**, 474 (2006).
[5] M. Arnould and S. Goriely, Phys. Rep. **384**, 1 (2003).
[6] H. Utsunomiya, P. Mohr, A. Zilges, and M. Rayet, Nucl. Phys. **A777**, 459 (2006).
[7] C. Angulo, M. Arnould, M. Rayet, P. Descouvemont, D. Baye, C. Leclercq-Willain, A. Coc, S. Barhoumi, P. Aguer, C. Rolfs *et al*., Nucl. Phys. **A656**, 3 (1999).
[8] Gy. Gyürky, Zs. Fülöp, E. Somorjai, M. Kokkoris, S. Galanopoulos, P. Demetriou, S. Harissopulos, T. Rauscher, and S. Goriely, Phys. Rev. C **68**, 055803 (2003).
[9] Gy. Gyürky, E. Somorjai, Zs. Fülöp, S. Harissopulos, P. Demetriou, and T. Rauscher, Phys. Rev. C **64**, 065803 (2001).
[10] S. Galanopoulos, P. Demetriou, M. Kokkoris, S. Harissopulos, R. Kunz, M. Fey, J. W. Hammer, Gy. Gyürky, Zs. Fülöp, E. Somorjai, and S. Goriely, Phys. Rev. C **67**, 015801 (2003).
[11] P. Tsagari, M. Kokkoris, E. Skreti, A. G. Karydas, S. Harissopulos, T. Paradellis, and P. Demetriou, Phys. Rev. C **70**, 015802 (2004).
[12] C. E. Laird, D. Flynn, R. L. Hershberger, and F. Gabbard, Phys. Rev. C **35**, 1265 (1987).
[13] S. Harissopulos, E. Skreti, P. Tsagari, G. Souliotis, P. Demetriou, T. Paradellis, J. W. Hammer, R. Kunz, C. Angulo, S. Goriely, and T. Rauscher, Phys. Rev. C **64**, 055804 (2001).
[14] T. Sauter and F. Käppeler, Phys. Rev. C **55**, 3127 (1997).
[15] F. R. Chloupek, A. St. J. Murphy, R. N. Boyd, A. L. Cole, J. Görres, R. T. Güray, G. Raimann, J. J. Zack, T. Rauscher, J. V. Schwarzenberg, P. Tischhauser, and M. Wiescher, Nucl. Phys. **A652**, 391 (1999).
[16] J. Bork, H. Schatz, F. Käppeler, and T. Rauscher, Phys. Rev. C **58**, 524 (1998).
[17] N. Özkan, A. St. J. Murphy, R. N. Boyd, A. L. Cole, R. deHaan, M. Famiano, J. Görres, R. T. Güray, M. Howard, L. Sahin, and M. Wiescher, Nucl. Phys. **A688**, 459c (2001).
[18] Gy. Gyürky, G. G. Kiss, Z. Elekes, Zs. Fülöp, and E. Somorjai, Eur. Phys. J. A **27**, s01, 141 (2006).
[19] Zs. Fülöp, Gy. Gyürky, and E. Somorjai, Nucl. Phys. **A758**, 90c (2005).
[20] N. Özkan, in *Proceedings of International Symposium on Nuclear Astrophysics-Nuclei in the Cosmos–IX, 25–30 June 2006*, PoS(NIC-IX)154, http://pos.sissa.it//archive/conferences/028/154/NIC-IX_154.pdf.
[21] M. S. Basunia, E. B. Norman, H. A. Shugart, A. R. Smith, M. J. Dolinski, and B. J. Quiter, Phys. Rev. C **71**, 035801 (2005).
[22] Zs. Fülöp, A. Z. Kiss, E. Somorjai, C. E. Rolfs, H. P. Trautvetter, T. Rauscher, and H. Oberhummer, Z. Phys. A **355**, 203 (1996).
[23] W. Rapp, M. Heil, D. Hentschel, F. Käppeler, R. Reifarth, H. J. Brede, H. Klein, and T. Rauscher, Phys. Rev. C **66**, 015803 (2002).
[24] Gy. Gyürky, G. G. Kiss, Z. Elekes, Zs. Fülöp, E. Somorjai, A. Palumbo, J. Görres, H. Y. Lee, W. Rapp, M. Wiescher, N. Özkan, R. T. Güray, G. Efe, and T. Rauscher, Phys. Rev. C **74**, 025805 (2006).
[25] N. Özkan, A. St. J. Murphy, R. N. Boyd, A. L. Cole, M. Famiano, R. T. Güray, M. Howard, L. Sahin, J. J. Zack, R. deHaan, J. Görres, M. C. Wiescher, M. S. Islam, and T. Rauscher, Nucl. Phys. **A710**, 469 (2002).
[26] S. Harissopulos, A. Lagoyannis, A. Spyrou, Ch. Zarkadas, G. Galanopoulos, G. Perdikakis, H.-W. Becker, C. Rolfs *et al*., J. Phys. G: Nucl. Part. Phys. **31**, S1417 (2005).
[27] E. Somorjai, Zs. Fülöp, A. Z. Kiss, C. E. Rolfs, H. P. Trautvetter, U. Greife, M. Junker, S. Goriely, M. Arnould, M. Rayet, T. Rauscher, and H. Oberhummer, Astron. Astrophys. **333**, 1112 (1998).
[28] D. Galaviz, Zs. Fülöp, Gy. Gyürky, Z. Mate, P. Mohr, T. Rauscher, E. Somorjai, and A. Zilges, Phys. Rev. C **71**, 065802 (2005); private communication (2006).

[29] T. Rauscher and F. K. Thielemann, At. Data Nucl. Data Tables **79**, 47 (2001).
[30] N. Özkan, G. Efe, R. T. Güray, A. Palumbo, M. Wiescher, J. Görres, H.-Y. Lee, Gy. Gyürky, E. Somorjai, and Zs. Fülöp, Eur. Phys. J. A **27**, s01, 145 (2006).
[31] R. B. Firestone and V. S. Shirley, *Table of Isotopes*, 8th ed. (Wiley, New York, 1996).
[32] http://www.nndc.bnl.gov/nudat2/indx-dec.jsp.
[33] S. Dababneh, N. Patronis, P. A. Assimakopoulos, J. Görres, M. Heil, F. Käppeler, D. Karamanis, S. O'Brien, and R. Reifarth, Nucl. Instrum. Methods A **517**, 230 (2004).
[34] K. Debertin and R. G. Helmer, *Gamma and X-ray Spectrometry with Semiconductor Detectors* (North-Holland, Amsterdam, 1989).
[35] F. J. Shima and D. D. Hoppea, Int. J. Appl. Radiat. Isotopes **38**, 1109 (1983).
[36] L. McFadden and G. R. Satchler, Nucl. Phys. **84**, 177 (1966).
[37] M. Avrigeanu, W. von Oertzen, A. J. M. Plomben, and V. Avrigeanu, Nucl. Phys. **A723**, 104 (2003).
[38] T. Rauscher, Nucl. Phys. **A719**, 73c (2003).
[39] P. Demetriou, C. Grama, and S. Goriely, Nucl. Phys. **A707**, 253 (2002).